Osmotically driven flows in microchannels separated by a semipermeable membrane

Kåre Hartvig Jensen,[a] Jinkee Lee,[b] Tomas Bohr[c] and Henrik Bruus†*[a]

Received 24th October 2008, Accepted 25th March 2009
First published as an Advance Article on the web 20th April 2009
DOI: 10.1039/b818937d

We have fabricated lab-on-a-chip systems with microchannels separated by integrated membranes allowing for osmotically driven microflows. We have investigated these flows experimentally by studying the dynamics and structure of the front of a sugar solution travelling in 200 μm wide and 50–200 μm deep microchannels. We find that the sugar front travels at a constant speed, and that this speed is proportional to the concentration of the sugar solution and inversely proportional to the depth of the channel. We propose a theoretical model, which, in the limit of low axial flow resistance, predicts that the sugar front should indeed travel with a constant velocity. The model also predicts an inverse relationship between the depth of the channel and the speed, and a linear relation between the sugar concentration and the speed. We thus find good qualitative agreement between the experimental results and the predictions of the model. Our motivation for studying osmotically driven microflows is that they are believed to be responsible for the translocation of sugar in plants through the phloem sieve element cells. Also, we suggest that osmotic elements can act as on-chip integrated pumps with no movable parts in lab-on-a-chip systems.

I. Introduction

Osmotically driven flows are believed to be responsible for the translocation of sugar in plants, a process that takes place in the phloem sieve element cells.[1] These cells form a micro-fluidic network which spans the entire length of the plant measuring from 10 μm in diameter in small plants to 100 μm in diameter in large trees.[1] The mechanism driving these flows is believed to be the osmotic pressures that build up relative to the neighboring water-filled tissue in response to loading and unloading of sugar into and out of the phloem cells in different parts of the plant.[1] This mechanism, collectively called the pressure-flow hypothesis, is much more efficient than diffusion, since the osmotic pressure difference caused by a difference in sugar concentration creates a bulk flow directed from large concentrations to small concentrations, in accordance with the basic needs of the plant.

Experimental verification of flow rates in living plants is difficult,[2] and the experimental evidence from artificial systems backing the pressure-flow hypothesis is scarce and consists solely of results obtained with centimetric sized setups.[3–5] However, many theoretical and numerical studies of the sugar translocation in plants have used the pressure-flow hypothesis[6–8] with good results. To verify that these results are indeed valid, we believe that it is of fundamental importance to conduct a systematic survey of osmotically driven flows at the micrometre scale. Finally, osmotic flows in microchannels can act as migration enhancers[9] or as microscale on-chip pumps with no movable parts. Examples of previous off-chip osmotic pumps are the device developed by Park *et al.*[10] and the osmotic pills developed by Shire Laboratories and pioneered by Theeuwes.[11] Also, there is a direct analogy between osmotically driven flows powered by concentration gradients, and electroosmotically driven flows in electrolytes[12,13] powered by electrical potential gradients.

II. Experimental setup

A. Chip design and fabrication

To study osmotically driven flows in microchannels, we have designed and fabricated a microfluidic system consisting of two layers of 1.5 mm thick polymethyl methacrylate (PMMA) separated by a semipermeable membrane (Spectra/Por Biotech Cellulose Ester dialysis membrane, MWCO 3.5 kDa, thickness ~40 μm), as sketched in Fig. 1(a)–(d). Channels of length 27 mm, width 200 μm and depth 50–200 μm were milled in the two PMMA layers by use of a MiniMill/Pro3 milling machine.[14,15] The top channel contains partly the sugar solution, and partly pure water, while the bottom channel always contains only pure water. To facilitate the production of a steep concentration gradient by cross-flows, a 200 μm wide cross-channel was milled in the upper PMMA layer perpendicular to and bi-secting the main channel. Inlets were produced by drilling 800 μm diameter holes through the wafer and inserting brass tubes into these. By removing the surrounding material, the channel walls in both the top and bottom layers acquired a height of 100 μm and a width of 150 μm. After assembly, the two PMMA layers were positioned such that the main channels in either layer were facing each other. Thus, when clamping the two layers together using two

[a]*Center for Fluid Dynamics, Department of Micro- and Nanotechnology, Technical University of Denmark, DTU Nanotech Building 345 East, DK-2800 Kongens Lyngby, Denmark*
[b]*School of Engineering and Applied Science, Harvard University, Cambridge, Massachusetts, 02138, USA*
[c]*Center for Fluid Dynamics, Department of Physics, Technical University of Denmark, DTU Physics Building 309, DK-2800 Kongens Lyngby, Denmark*
† *E-mail:* bruus@nanotech.dtu.dk

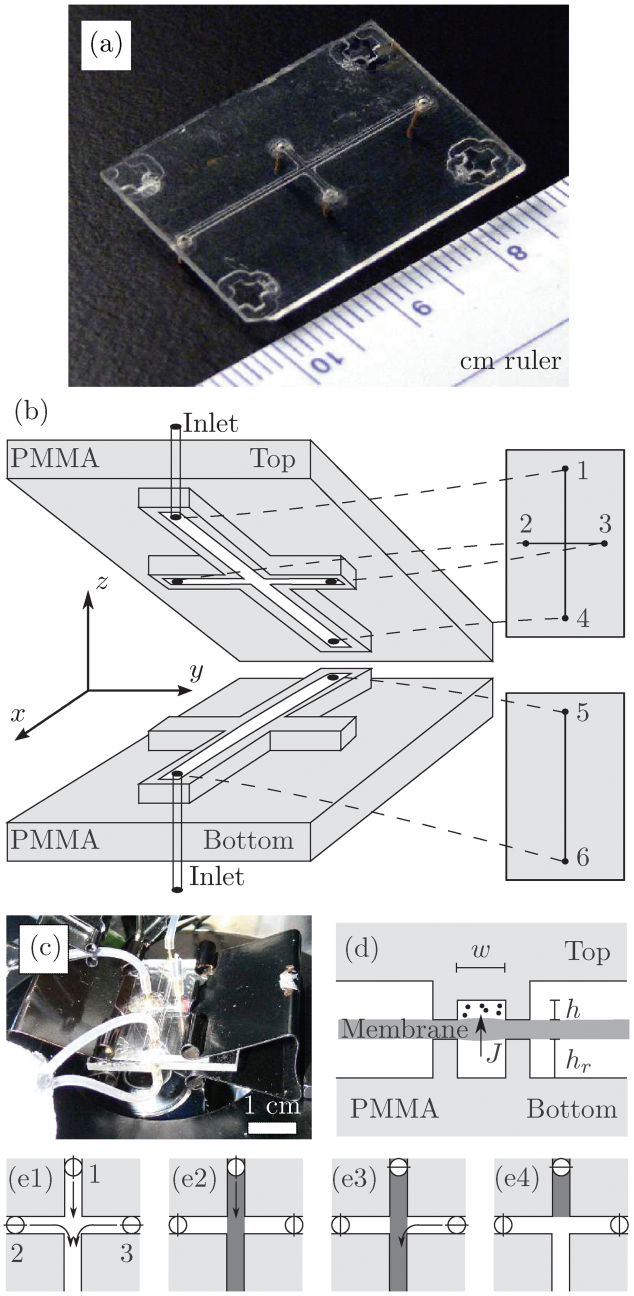

Fig. 1 (a) Picture of the top part (upside down) of the chip showing the elevated channel and the four brass inlet tubes (pointing down). The crosses in the four corners were used for alignment. (b) Schematics of the two PMMA layers (gray) showing the elevated channels (white) facing each other. All six inlet positions (black dots) are marked, but for clarity only two brass tubes are shown. (c) Picture of the fully assembled setup. (d) Schematic cross-section close-up of the two PMMA layers (gray) clamped together with the semipermeable membrane (dark gray) in between. The sugar in the upper channel (black dots) and the water influx J from the lower channel (arrow) are also marked. (e1)–(e4) Valve settings (circles) and cross-flow flushing procedure (arrows) for creating a sharp front in the top channel between the sugar/dye solution (dark gray) and the pure water (white). See details in the text.

30 mm paper clamps, the membrane acted as a seal, stopping any undesired leaks from the channels as long as the applied pressure did not exceed approximately 1 bar.

B. Measurement setup and procedures

In our setup, the osmotic pressure pushes water from the lower channel, through the membrane, and into the sugar-rich part of the upper channel. This displaces the solution along the upper channel thus generating a flow there, as shown in Fig. 2. To measure this flow inside the upper channel, particle and dye tracking were used. In both cases inlets 1, 2, 3 and 5 (see Fig. 1) were connected *via* silicone tubing (inner diameter 0.5 mm) to disposable syringes. Syringes 2, 3 and 5 were filled with demineralised water and syringe 1 was filled with a solution of sugar (sucrose or dextran (mol. weight: 17.5 kDa, Sigma-Aldrigde, type D4624)) and 5% volume red dye (Flachsmann Scandinavia, Red Fruit Dye, type 123000) in the dye tracking experiments and 0.05% volume sulfate modified 1 μm polystyrene beads (Sigma-Aldrigde, L9650-1ML, density 1050 kg m^{-3}) in the particle tracking experiments. Inlets 4 and 6 were connected to the same water bath to minimize the hydrostatic pressure difference between the two sides of the membrane. The liquid height in the water bath was carefully aligned to the top channel to avoid any difference in liquid height that might have resulted in a flow in the opposite direction. When conducting both dye tracking and particle tracking experiments, the initialization procedure shown in Fig. 1(e1)–(e4) was used: first (e1), inlet valves 1, 2 and 3 were opened and all channels were flushed thoroughly with pure water (white) to remove any air bubbles and other impurities. Second (e2), after closing inlets 2 and 3 a sugar solution (dark gray) was injected through inlet 1 filling the main channel in the upper layer. Third (e3), inlet 1 was closed and water was carefully pumped through inlet 2 to produce a sharp concentration front at the cross, as shown in Fig. 1(e4) and 3(b).

1. Sugar front motion recorded by dye tracking. The motion of the sugar front in the upper channel was recorded by taking pictures of the channel in 10 s intervals using a Leica MZ 16 microscope. This yielded images as those displayed in Fig. 3(a), clearly showing a front (marked by arrows) of the sugar/dye solution moving along the channel. To obtain the position $\lambda(t)$ of the sugar front as a function of time t, the distance from the initial front position λ_0 to the current position $\lambda(t)$ was measured using ImageJ software. The position of the sugar front was taken to be at

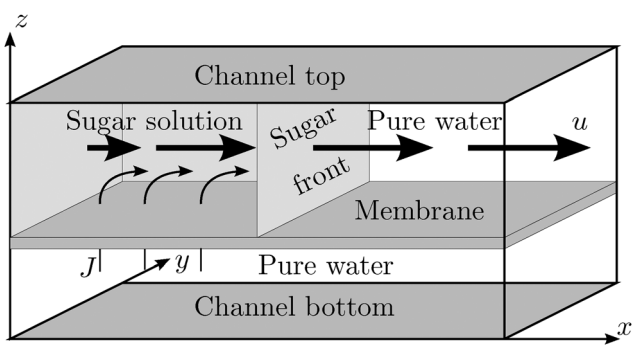

Fig. 2 A sketch of the osmotically driven flow. The osmotic pressure forces water from the lower channel, through the membrane, and into the sugar-rich part (light gray region) of the upper channel. The water flux J (curved arrows), which pushes the sugar front forward, is related to the sugar concentration by eqn (3). The resulting flow velocity u is represented by the thick horizontal arrows.

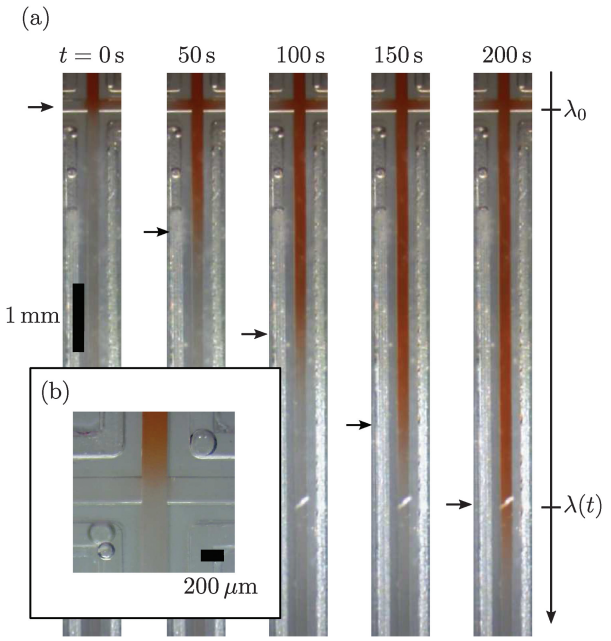

Fig. 3 (a): Images showing the sugar front moving in the 200 μm × 200 μm channel. The time between each image is 50 s. The arrows indicate the position of the sugar front as it moves down along the channel. (b): Closeup of the cross junction just after a sharp sugar/water interface has been created.

the end of the highly saturated dark region. In this way, the position of the front could be measured at each time step with an accuracy of ±200 μm. As verified in earlier works,[3,5] we assumed that the sugar and dye travelled together, which is reasonable since the Péclet number (Pé) is ~10 (see Section 4). Experiments with dye alone were carried out. These showed, that the osmotic pumping due to the dye molecules was negligible. We only applied the dye tracking method on the 200 μm deep channel, since the 100 μm and 50 μm deep channels were too shallow for sufficient scattering of red light by the solution to get a clear view of the front.

2. Sugar front motion recorded by use of particle tracking. The flow velocity inside the upper channel was recorded by tracking the motion of 1 μm beads in the water 3 mm ahead of the initial sugar front position. Images were recorded every 200–1000 ms for up to 400 s using a Unibrain Fire-i400 1394 digital camera attached to a Nikon Diaphot microscope with the focal plane at $h/2$ and a focal depth of approximately 10 μm. Sedimentation times for the particles were 1800 s for the 200 μm channel and 450 s for the 50 μm channel. Since only the first 150 s were used when determining the front velocity, this did not interfere with our measurements. At the point of observation, well ahead of the front, the flow behaved as if it were pressure driven (see the insert in Fig. 5) and the standard laminar flow profile[18] was used to determine the average flow velocity.

III. Experimental results

A. Dye tracking

Fig. 4 shows the position of the sugar front in the 200 μm deep channel as a function of time obtained by dye tracking. The data sets correspond to different concentrations of sucrose and dextran as indicated in the legends. Initially, the sugar front moves with constant speed, but then it gradually decreases, more so for low than high concentrations. The solid black lines are linear fits for the first 100 s giving the initial velocity of the front. As a function of time the front smears out over a region of growing width w_f. In Fig. 4(c) w_f is plotted *vs.* time for the

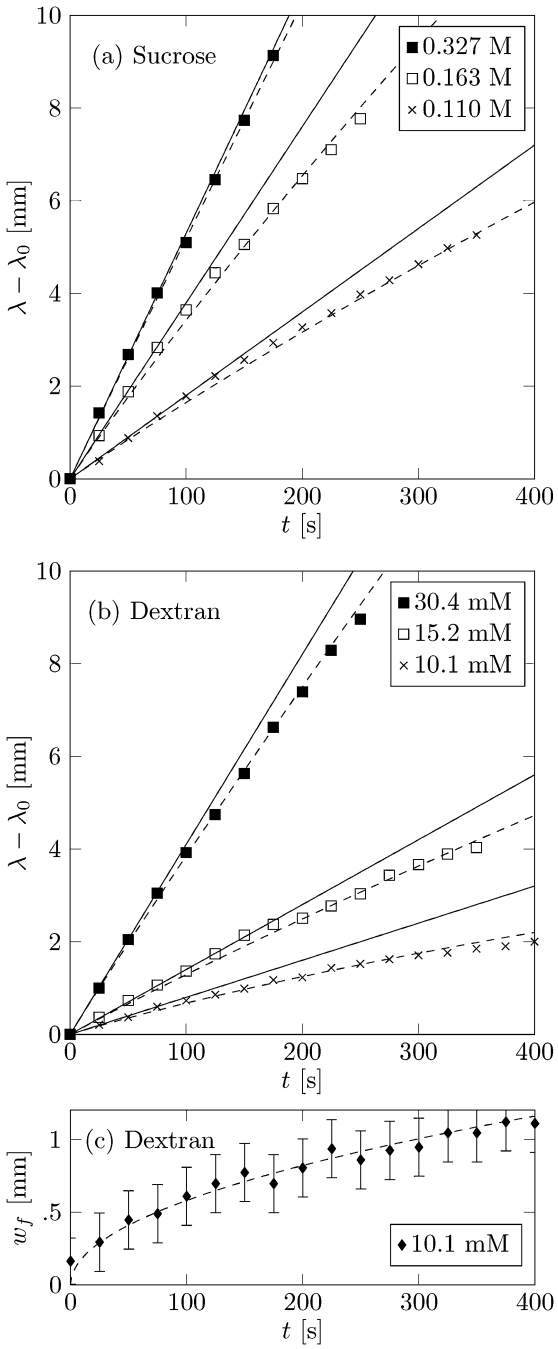

Fig. 4 Measured position λ of the sugar front as a function of time t in the 200 μm × 200 μm channel for various concentrations of (a) sucrose and (b) dextran. The solid black lines are linear fits for $0\ s < t < 100\ s$. The dashed lines are fits to eqn (13). (c) The width w_f of the sugar front as a function of time for the 10.1 mM dextran experiment. The dashed black line is a fit to $(2Dt)^{1/2}$ with $D = 1.7 \times 10^{-9}$ m^2 s^{-1}, 5 times larger than the value given in Table I. This, however, is in good agreement with the Taylor dispersion theory,[19,20] since Pé ≃ 15.

Table 1 List of parameters in alphabetic order after the symbol

Parameter	Symbol	Value and/or unit
Sugar concentration	c	mol L^{-1}
Initial concentration	c_0	mol L^{-1}
Diffusive concentration loss	Δc	mol L^{-1}
Diffusion constant	D	m^2 s^{-1}
Sucrose, see Ref. 16	D	4.6×10^{-10} m^2 s^{-1}
Dextran, see Ref. 5	D	7.0×10^{-11} m^2 s^{-1}
Dye, see Ref. 16	D	3.4×10^{-10} m^2 s^{-1}
Height of channel	h	50, 100, 200 μm
Height of reservoir	h_r	200 μm
Flux across membrane	J	m s^{-1}
Length of channel	L	27 mm
Membrane permeability	L_p	1.8 pm $(Pa\ s)^{-1}$
Diffusion length	l_D	m
Münch number	M	
Hydrostatic pressure	p	Pa
Péclet number, local	Pé	
Péclet number, global	$Pé_g$	
Gas constant	R	8310 Pa L $(K\ mol)^{-1}$
Position of sugar front	s	
Absolute temperature	T	K
Time	t	s
x-Velocity of sugar front	U	m s^{-1}
Mean x-velocity of sugar front	u	m s^{-1}
Volume behind sugar front	V	m^3
Width of channel	w	200 μm
Width of sugar front	w_f	m
Cartesian coordinates	x, y, z	m
Osmotic coefficients:		
Dextran ($T = 293$ K)	α	41, see Ref. 5
Sucrose ($T = 293$ K)	α	1, see Ref. 17
Fitting parameter	δ	m^2 s^{-1}
Viscosity	η	Pa s
Position of sugar front	λ	m
Position of initial sugar front	λ_0	13.5 mm
Osmotic pressure	Π	Pa

10.1 mM dextran experiment along with a fit to $w_f = (2Dt)^{1/2}$ showing that the sugar front broadens by molecular diffusion. Here, D is the molecular diffusion constant.

B. Particle tracking

Fig. 5 shows the velocity as a function of time obtained by particle tracking in a 200 μm × 200 μm channel. For the first 150 s the velocity is approximately constant after which it starts decreasing as the sugar front passes the point of observation. We interpret the mean value of the initial plateau of the velocity graph as the speed of the sugar front. Fig. 6(a) and (b) shows the velocity of the sugar front as a function of dextran concentration and of channel depth obtained in this way.

IV. Theoretical analysis

When modeling the flow inside the channel, we use an approach similar to that of Eschrich *et al.*[3] They introduced a 1D model with no axial flow resistance and zero diffusivity in a setting very similar to ours. To formalize this, we consider the two most important non-dimensional numbers in the experiments: the Münch number[5] M and the Péclet number Pé.[18] These numbers characterize the ratio of axial to membrane flow resistance and axially convective to diffusive fluxes respectively. In our experiments

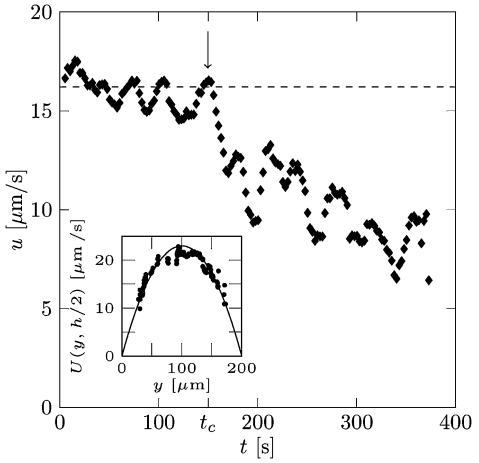

Fig. 5 The average flow velocity u in the 200 μm deep channel as a function of time t measured 3 mm ahead of the initial front position. At $t_c \simeq 150$ s (indicated by the arrow), the sugar front begins to reach the observation point, and the velocity decreases rapidly. For $t > t_c$, the velocity was not determined accurately. The insert shows a typical velocity profile $U(y, h/2)$ in the center plane across the 200 μm × 200 μm channel obtained by particle tracking. The solid black line is a fit to the velocity profile for a rectangular channel used when obtaining the average flow velocity.

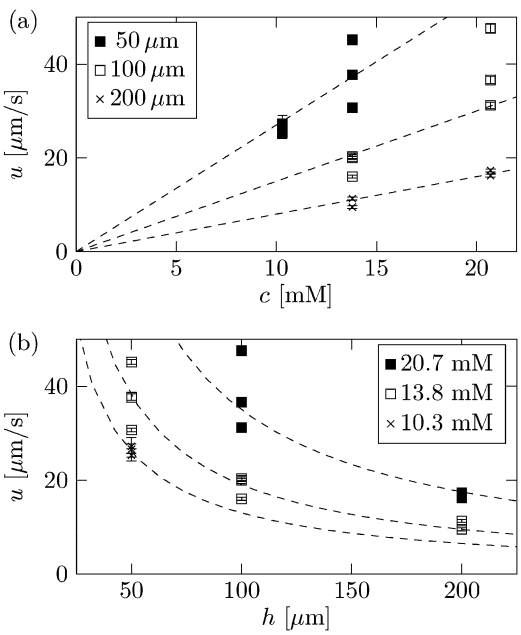

Fig. 6 Front velocity u obtained by particle tracking. (a) The velocity u plotted against dextran concentration c_0. The dashed lines are fits to c provided as guides to the eye. (b) The velocity u plotted against channel depth h. The dashed lines are fits to $1/h$ provided as guides to the eye.

$$M = \frac{wLL_p\,\alpha RTc}{\frac{wh^3}{\eta L}\alpha RTc} = \frac{\eta L^2 L_p}{h^3} \sim 10^{-6} \tag{1}$$

and

$$Pé = \frac{w_f u}{D} \sim 10 \tag{2}$$

Here η is the viscosity (typically 1.5 mPa s), w_f is the width of the sugar front (typically 500 μm), and D the molecular diffusivity of sugar (typically 10^{-10} m^2 s^{-1} for sucrose and the dye and 10^{-11} m^2 s^{-1} for dextran)

A. Equation of motion

Since $M \ll 1$ and Pé $\gg 1$, we shall neglect the axial flow resistance and the diffusion of the sugar in our analysis. In this way, let $\lambda(t)$ denote the position of the sugar/dye front in the upper channel, and let V denote the volume behind the front. The flux J of water across the membrane from the lower to the upper channel (see Fig. 1(d)), is given by

$$J = L_p(\Delta p + \Delta\Pi) \simeq L_p \alpha RTc \tag{3}$$

where L_p is the membrane permeability, Δp the hydrostatic and $\Delta\Pi$ the osmotic pressure difference across the membrane. In our experiments $\Delta p = 0$, and from the van 't Hoff relation follows $\Delta\Pi \simeq \alpha RTc$, where α is the osmotic non-ideality coefficient, R is the gas constant, T is the absolute temperature, and c is the concentration of sugar molecules. Since the concentration is independent of x behind the front and zero ahead of it, J is also independent of x. By the conservation of sugar this allows us as a first approximation to write the concentration as

$$c(x,t) = \begin{cases} c_0 \dfrac{\lambda_0}{\lambda(t)} & x \le \lambda(t) \\ 0 & x \ge \lambda(t) \end{cases} \tag{4}$$

Moreover, the rate of change of the expanding volume V behind the front can be related to J as

$$\begin{aligned} \frac{\mathrm{d}V}{\mathrm{d}t} &= w\int_0^L J(x)\mathrm{d}x \\ &= wL_p\alpha RTc_0\frac{\lambda_0}{\lambda(t)}\int_0^{\lambda(t)}\mathrm{d}x \\ &= w\lambda_0 L_p \alpha RTc_0 \end{aligned} \tag{5}$$

However, we also have that

$$\frac{\mathrm{d}V}{\mathrm{d}t} = hw\frac{\mathrm{d}\lambda(t)}{\mathrm{d}t} \tag{6}$$

which implies together with eqn (5) that

$$\lambda(t) = \lambda_0 + \frac{\lambda_0}{h}L_p\alpha RTc_0 t = \lambda_0 + ut \tag{7}$$

where the velocity u of the front is given by

$$u = \frac{\lambda_0}{h}L_p\alpha RTc_0 \tag{8}$$

B. Corrections to the equation of motion

In the previous section, we considered the motion of a sharp sugar front, as given by the stepwise concentration profile in eqn (4), and found that this moved with constant velocity. However, as can be seen in Fig. 4(a,b) the front velocity gradually decreases. To explain this, we consider two effects. First, we observe that in Fig. 3(a) there exists a region of growing size separating the sugar/dye-filled region from the region of pure water. Even though the sugar and the dye diffuse at different rates, we shall assume that some of the sugar also lies ahead of the visible front. Since the sugar in this region is located ahead of the front, the osmotic pumping in the observed volume behind the front is lowered, thus slowing down the motion of the observed front. Second, we note that sugar leaking across the membrane also lowers the osmotic pumping behind the front. This effect should be especially pronounced for sucrose, since its molecular weight is smaller than the cut-off of the membrane. Common to these two effects is, however, that they are driven by diffusion. In the first case, sugar diffuses from the pumping region to a region ahead of the front and in the second it diffuses across the membrane. The nature of these two effects makes them impossible to distinguish from one another. Lumping them together as one diffusion process characterized by an effective diffusion constant δ, we may rewrite eqn (4) as

$$c(x,t) = \begin{cases} c_0 \dfrac{\lambda_0}{\lambda(t)+\ell_D} & x \le \lambda(t) \\ 0 & x \ge \lambda(t) \end{cases} \tag{9}$$

where $\ell_D = (2\delta t)^{1/2}$. Here δ is a fitting parameter which has the dimension of a diffusion coefficient and which includes both of the effects mentioned above. In this way, the amount of sugar lost from the observed volume by diffusion is $\Delta c \simeq c_0(2\delta t)^{1/2}$, as indicated in Fig. 7.

Using eqn (5) and (6) the time derivative of λ becomes

$$\frac{\mathrm{d}\lambda}{\mathrm{d}t} = \frac{L_p\alpha RTc_0\lambda_0}{h}\frac{\lambda}{\lambda+\ell_D} \tag{10}$$

Rescaling using $\lambda = s\lambda_0$ and $t = \tau\dfrac{\lambda_0}{u}$, we get that

$$\frac{\mathrm{d}s}{\mathrm{d}\tau} = \frac{s}{s+\left(\frac{\tau}{\mathrm{Pé_g}}\right)^{1/2}} \tag{11}$$

where we have introduced the global Péclet number related to the loss of sugar by diffusion,

$$\mathrm{Pé_g} = \frac{2\lambda_0^2 L_p\alpha RTc_0}{\delta h} = \frac{2\lambda_0}{\delta}u \tag{12}$$

Given the experimental conditions, Pé$_g$ is typically of the order 10^1–10^2. Thus, for $\left(\frac{\tau}{\mathrm{Pé_g}}\right)^{1/2} \ll 1$, eqn (11) can be solved by an expansion,

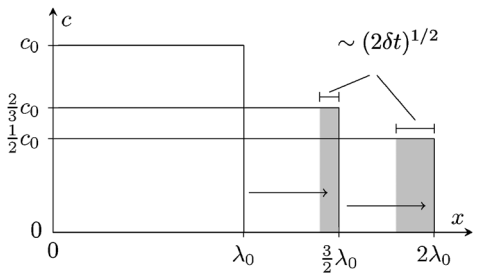

Fig. 7 The time evolution of the sugar concentration profile given by eqn (4). The gray regions represents the sugar lost from the observed region by diffusion, see eqn (9).

$$s = s_0 + \tau\left(1 - \frac{2}{3s_0}\left(\frac{\tau}{\mathrm{Pé_g}}\right)^{1/2} + O\left[\left(\frac{\tau}{\mathrm{Pé_g}}\right)\right]\right) \qquad (13)$$

We have made numerical simulations of the full 1D coupled velocity-concentration equation system for the special case of diffusion ahead of the front. Our results show, that the simple model in eqn (13) captures the essential dynamics of the motion of the sugar front. The dashed lines in Fig. 4(a) and (b) are fits to eqn (13), with values of δ varying between 2×10^{-7} m^2 s^{-1} and 4×10^{-9} m^2 s^{-1}, showing good qualitative agreement between theory and experiment. However, since we have not tracked the sugars directly, these cannot immediately be compared with the values for sucrose ($D = 4.6 \times 10^{-10}$ m^2 s^{-1}) and dextran ($D = 7.0 \times 10^{-11}$ m^2 s^{-1}). To completely resolve this issue, experiments with *e.g.* fluorescently tagged sugar molecules where the concentration on both sides of the membrane is measured are needed.

V. Discussion

A. Comparison of theory and experiment

To compare the experimental data with theory, we have in Fig. 8 plotted the empirically obtained velocities u_{exp} against those predicted by eqn (8). For nearly all the dextran and sucrose experiments we see a good agreement between experiment and theory, although eqn (8) systematically overestimates the expected velocities.

We interpret the quantitative disagreement as an indication of a decreasing sugar concentration in the top channel due to diffusion of sugar into the membrane as well as the presence of a low-concentration boundary layer near the membrane, a so-called unstirred layer.[21]

B. Osmotic pumps in lab-on-a-chip systems

Depending on the specific application, flows in lab-on-a-chip systems are conventionally driven by either syringe pumps or by using more advanced techniques such as off-chip osmotic pumps,[10] electronically controlled pressure devices, electro-osmotic pumps,[22] evaporation pumps,[23] or capillary pumps.[24]

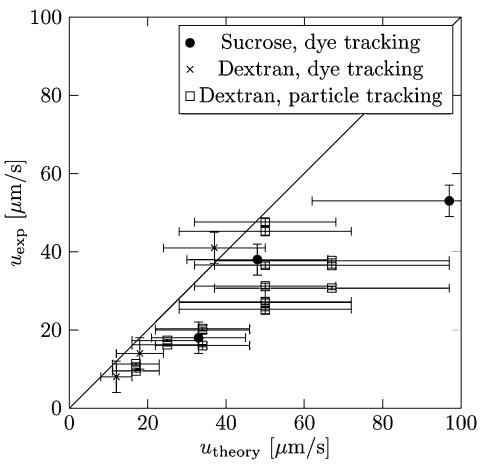

Fig. 8 The experimental values of the front velocity u_{exp} plotted against the theoretical results u_{theory} from eqn (8).

Most of these techniques involves the integration of either movable parts or complicated electronics into the lab-on-a-chip device. As an application of our design and fabrication method, we suggest the use of integrated osmotic pumps in lab-on-a-chip systems. This could be done by integrating in the device a region where the channel is in contact through a membrane with a large reservoir containing an osmotically active agent. By using a sufficiently large reservoir, say 1 cm^3, and a 100 μm × 100 μm channel with a flow rate of 100 μm s^{-1} it would take more than 10 days to reduce the reservoir concentration by 50% and thus decrease the pumping rate by 50%. We emphasize that such osmotic pumping would be completely steady, even at very low flow rates.

VI. Conclusions

We have studied osmotically driven, transient flows in 200 μm wide and 50–200 μm deep microchannels separated by a semi-permeable membrane integrated in a microfluidic PMMA chip. These flows are generated by the influx of water from the lower channel containing pure water, through the semipermeable membrane, into the large sugar concentration placed in one end of the top channel. We have observed that the sugar front in the top channel travels with constant speed, and that this speed is proportional to the concentration of the sugar solution and inversely proportional to the depth of the channel. We propose a theoretical model, which, in the limit of low axial flow resistance, predicts that the sugar front should travel with a constant velocity. The model also predicts an inverse relationship between the depth of the channel and the speed and a linear relation between the sugar concentration and the speed. We compare theory and experiment with good qualitative agreement, although the detailed mechanism behind the deceleration of the flow is still unknown. Finally, we suggest that on-chip osmotic elements can potentially act as pumps with no movable parts in lab-on-a-chip systems.

VII. Acknowledgements

It is a pleasure to thank Emmanuelle Rio, Christophe Clanet, Frederik Bundgaard, Jan Kafka and Oliver Geschke for assistance and advice on chip design and manufacturing. We also thank Alexander Schulz, Michele Holbrook, Maciej Zwieniecki and Howard Stone for many useful discussions of the biological and physical aspects of osmotically driven flows. This work was supported by the Danish National Research Foundation, Grant no. 74 and by the Materials Research Science and Engineering Center at Harvard University.

References

1 L. Taiz and E. Zeiger, *Plant Physiology* (Sinauer Associates, Inc., 2002), 3rd edn.
2 M. Knoblauch and A. J. E. van Bel, *Plant Cell*, 1998, **10**, 35.
3 W. Eschrich, R. F. Evert and J. H. Young, *Planta (Berl.)*, 1972, **107**, 279.
4 A. Lang, *J. Exp. Bot.*, 1973, **24**, 896.
5 K. Jensen, E. Rio, R. Hansen, C. Clanet and T. Bohr, *J. Fluid Mech.*, 2008, Submitted.
6 M. V. Thompson and N. M. Holbrook, *J. Theo. Biol.*, 2003, **220**, 419.
7 M. V. Thompson and N. M. Holbrook, *Plant, Cell Environ.*, 2003, **26**, 1561.
8 T. Hölttä, *Trees – Structure and Function*, 2006, **20**, 67.

9 B. Abecassis, C. Cottin-Bizonne, C. Ybert, A. Ajdari and L. Bocquet, *Nature Materials*, 2008, **7**, 785.
10 J. Y. Park, C. M. Hwang, S. H. Lee and S.-H. Lee, *Lab Chip*, 2007, **7**, 1673.
11 F. Theeuwes, *J. Pharm. Sci.*, 1975, **64**, 1987.
12 A. Brask, J. Kutter and H. Bruus, *Lab Chip*, 2005, **5**, 730.
13 M. Gregersen, L. Olesen, A. Brask, M. Hansen and H. Bruus, *Phys. Rev. E*, 2007, **76**, 056305.
14 O. Geschke, *Microsystem Engineering of Lab-on-a-Chip Devices* (Wiley-VCH, 2004).
15 F. Bundgaard, G. Perozziello and O. Geschke, *Proceedings of the Institution of Mechanical Engineers Series C*, 2007, **220**, 1625.
16 P. Atkins, *Physical Chemistry* (Oxford University Press, 1978).
17 B. E. Michel, *Plant Physiol.*, 1972, **50**, 196.
18 H. Bruus, *Theor. Microfluid.* (Oxford University Press, 2008).
19 G. I. Taylor, *Proc. Roy. Soc. A*, 1953, **291**, 186.
20 J. Lee, E. Kulla, A. Chauhan and A. Tripathi, *Phys. Fluids*, 2008, **20**, 093601.
21 T. J. Pedley, *Quarterly Review of Biophysics*, 1983, **16**, 115.
22 A. Ajdari, *Phys. Rev. E*, 2000, **61**, R45.
23 X. Noblin, L. Mahadevan, I. A. Coomaraswamy, D. A. Weitz, N. M. Holbrook and M. A. Zwieniecki, *PNAS*, 2008, **105**, 9140.
24 S. Boudait, O. Hansen, H. Bruus, C. Berendsen, N. Bau-Madsen, P. Thomsen, A. Wolff and J. Jonsmann, *Lab Chip*, 2005, **5**, 827.